Statistical Analysis of Modal Dispersion in Field-Installed Coupled-Core Fiber Link

Martina Cappelletti, *Member, OSA*, Mikael Mazur, *Member, IEEE, Member, OSA*, Nicolas K. Fontaine, *Senior Member, IEEE, Fellow, OSA*, Roland Ryf, *Fellow, IEEE, Fellow, OSA*, Tetsuya Hayashi, *Senior Member, IEEE*, Antonio Mecozzi, *Fellow, IEEE, Fellow, OSA*, Marco Santagiustina, *Member, IEEE*, Andrea Galtarossa, *Fellow, IEEE, Fellow, OSA*, Cristian Antonelli, *Senior Member, IEEE, Fellow, OSA*, and Luca Palmieri, *Senior Member, IEEE*

(Top-Scored Paper)

***Abstract*—This article presents a statistical analysis of modal dispersion of a 69-km-long field-deployed coupled-core four-core fiber link. The link is characterized over a band of approximately 5 THz at 1550 nm, in terms of complex modal dispersion vector, eigenvalues of its modal dispersion matrix, and intensity impulse response. Experimental statistical results are in very good agreement with the theoretical models based on the assumption of strong mode mixing. We also show that a careful analysis of the modal dispersion vector enables the accurate assessment of the skew between channels, distinguishing the contribution of the input patch cords from that of the output ones. Notably, we show that the Stokes-space representation of modal dispersion allows to compensate for the delays introduced at the fiber input and output by the optical vector network analyzer used for measurements. In addition, we provide evidence and theoretical justification of spectral persistence of the principal states in fibers with strong mode mixing. That is, although the modal content and the group delays of the principal modes change from frequency to frequency, the sorting of the principal modes with respect to their group delays is largely frequency independent.**

Manuscript received 30 November 2023; revised 26 January 2024; accepted 29 January 2024. Date of publication 1 February 2024; date of current version 14 June 2024. This work was supported in part by the European Union through the Italian National Recovery and Resilience Plan (NRRP) of NextGenerationEU, partnership on "Telecommunications of the Future" (PE0000001 - Program RESTART) and in part by (MIUR PRIN 2017, project FIRST). *(Corresponding author: Martina Cappelletti.)*

Martina Cappelletti is with the Department of Information Engineering, University of Padova, 35131 Padova, Italy (e-mail: martina.cappelletti.1@phd.unipd.it).

Mikael Mazur, Nicolas K. Fontaine, and Roland Ryf are with Nokia Bell Labs, Crawford Hill, NJ 07733 USA (e-mail: mikael.mazur@nokia-bell-labs.com; nicolas.fontaine@nokia-bell-labs.com; roland.ryf@nokia-bell-labs.com).

Tetsuya Hayashi is with Sumitomo Electric Industries, Ltd., Kanagawa 244-8588, Japan (e-mail: t-hayashi@sei.co.jp).

Antonio Mecozzi and Cristian Antonelli are with the Department of Physical and Chemical Sciences, University of L'Aquila, 67100 L'Aquila, Italy, and also with the National Inter-University Consortium for Telecommunications - CNIT, 43124 Parma, Italy (e-mail: antonio.mecozzi@univaq.it; cristian.antonelli@univaq.it).

Marco Santagiustina, Andrea Galtarossa, and Luca Palmieri are with the Department of Information Engineering, University of Padova, 35131 Padova, Italy, and also with the National Inter-University Consortium for Telecommunications - CNIT, 43124 Parma, Italy (e-mail: marco.santagiustina@unipd.it; andrea.galtarossa@dei.unipd.it; luca.palmieri@dei.unipd.it).

Color versions of one or more figures in this article are available at https://doi.org/10.1109/JLT.2024.3361088.

Digital Object Identifier 10.1109/JLT.2024.3361088

***Index Terms*—Modal dispersion, coupled-core fiber, skew, group delays, field-deployed MCF, intensity impulse response, SDM.**

I. Introduction

THE fiber-optic communications industry is on the brink of reaching its maximum capacity [1], leading to a pressing need for new and scalable technologies. One promising solution to this problem is space division multiplexing (SDM) transmission [2], which exploits multi-core fibers (MCFs) [3] and multi-mode fibers (MMFs) [4]. SDM utilizes multiple-input multiple-output (MIMO) techniques that rely on electronic digital signal processing (DSP). In order to design effective MIMO-DSP algorithms, it is crucial to understand the statistical aspects of signal propagation in SDM links. Modal dispersion (MD) and mode-dependent loss (MDL) are two critical factors that influence SDM transmission systems. Several models have been proposed to assess their impact on system performance [5], [6]. A recent study [7] presented a unified model, which considers the effects of both MD and MDL on the intensity impulse response (IIR) of the system. This work focuses on scenarios commonly found in coupled-core MCFs, where all modes undergo random coupling during propagation [8]. By employing a Stokes-space representation of multi-mode propagation, the model investigates how MD and MDL accumulate along the link and describes their influence on the IIR [9] of the system. The duration of the IIR determines the memory requirements for a MIMO-SDM receiver, and the model reveals its correlation with the root mean square value of the group delay.

Despite their relevance, the statistical models for SDM fiber systems have only been validated through numerical simulations or experiments conducted on spooled fibers. Extending previously reported preliminary results [10], this article introduces a significant contribution by presenting the first statistical analysis of experimental data obtained from a field-deployed SDM fiber link. Our findings demonstrate a very good agreement with the theoretical predictions, establishing a solid basis for the random coupling model of SDM fiber links. In particular, a major limitation of the analysis presented in [7] was that modal dispersion was characterized based on the overall SDM transmission

matrix estimated for the purpose of digital equalization, which prevented the isolation of the contribution of the multi-core fiber alone. The present work is in sharp contrast with this situation, as we use direct measurements of the transfer matrix of a field-deployed fiber obtained with an optical vector network analyzer (OVNA). The fiber under test is part of the SDM testbed deployed in the city of L'Aquila, in Italy [11].

II. Theoretical Description of Modal Dispersion and Skew

The light propagation in a fiber that supports $2\,N$ modes, considering polarization degeneracy, is described by the field vector $\vec{E}(z,\omega)$, which is constructed by stacking the complex spectra of the $2\,N$ individual modes. The linear propagation of light through the fiber can be described by the equation $\vec{E}(L,\omega) = \mathbf{F}(L,\omega)\vec{E}(0,\omega)$, where $\mathbf{F}(L,\omega)$ is the transfer matrix of the fiber link, and L denotes the length of the fiber. To simplify the notation, we omit the dependence on L in the following. Neglecting scalar factors common to all modes, the frequency dependence of $\mathbf{F}$ is given by [7]:

$$\frac{\partial \mathbf{F}(\omega)}{\partial \omega} = i\mathbf{Q}(\omega)\mathbf{F}(\omega). \tag{1}$$

The matrix $\mathbf{Q}$, also known as the modal dispersion matrix, has eigenvectors representing the principal modes of propagation (PMPs), while the eigenvalues are the relative delays of propagation of the PMPs [12]. In the presence of MDL, the eigenvalues are complex-valued. Specifically, the real part of the eigenvalues corresponds to the modal group delay (GD), while the imaginary part quantifies the corresponding loss. The MD matrix $\mathbf{Q}$ can be expressed as

$$\mathbf{Q}(\omega) = \frac{\vec{\tau}(\omega)\cdot\vec{\mathbf{\Lambda}}}{2\,N}, \tag{2}$$

where the elements of the vector $\vec{\mathbf{\Lambda}}$ are the generalized Pauli matrices $\mathbf{\Lambda}_n$, and $\vec{\tau}$ is the complex-valued MD vector [7], whose $D = 4\,N^2 - 1$ components are given by

$$\tau_n(\omega) = \text{Trace}\{\mathbf{\Lambda}_n\mathbf{Q}(\omega)\}. \tag{3}$$

The complex MD vector $\vec{\tau}$ extends the complex polarization-mode dispersion (PMD) vector [13] to the multi-mode case, taking into account the effect of both MD and MDL. In the absence of MDL, $\vec{\tau}$ becomes a real-value vector.

A. Analysis of Deterministic Skews

Despite the interpretation of the MD vector $\vec{\tau}(\omega)$ is not straightforward, it can be shown that its elements are either equal to differential group delays among modes, or equal to a linear combination of these delays. In the strong coupling regime, $\vec{\tau}(\omega)$ exhibits highly random behavior with respect to frequency, and its elements have in principle average equal to zero [7]. Therefore, any deterministic skew present in the link contributes to a non-zero average value of some of the MD vector components. Noticeably, as shown below, scalar skews arising from factors like single-mode patch-cords are represented by the last $N-1$ components of $\vec{\tau}$. Similarly, polarization skews originating from high birefringence elements present in the link are represented by the first $3\,N$ components of $\vec{\tau}$.

Scalar skews can be caused by single-mode patch-cords, such as those of spatial multiplexers. These patch-cords are too short to induce chromatic dispersion or PMD, therefore they are described by the diagonal matrix

$$\mathbf{M} = \text{diag}\left[\exp\left(-i\omega\mathbf{t}\right)\right], \text{ with } \mathbf{t} = [t_1, t_1, t_2, t_2, \ldots, t_N, t_N], \tag{4}$$

where t_n is the scalar delay induced on the nth spatial mode. Direct calculations show that the only non-zero elements of the MD vector $\vec{\tau}_M$, associated with the matrix $\mathbf{M}$, are the last $N-1$ ones, which are related to the delays t_i through the linear relation $(k = 1, \ldots, N-1)$

$$\tau_{4\,N^2-N+k} = \sqrt{\frac{4\,N}{k(k+1)}} \times \left(\sum_{n=1}^{N-1} t_n - k t_N\right), \tag{5}$$

Hence, with knowledge of the last $N-1$ elements of $\vec{\tau}_M$, it is possible to calculate the N delays, barring a common delay. By arbitrarily setting $t_1 = 0$ as a reference, the $N-1$ skews with respect to the first spatial mode can be obtained.

Polarization skews, i.e., differential delays between the polarization modes of a single spatial mode, are more easily identified in the MD vector. Intra-mode polarization effects are described by the N sub-matrices of size 2×2 on the diagonal of the transfer matrix $\mathbf{M}$. These sub-matrices correspond to the first N blocks of dimension 3 of the MD vector. Therefore, these 3-dimensional blocks are proportional to the PMD vectors associated with the corresponding spatial mode. In particular, the PMD of the nth spatial mode $\Delta\tau_n$ is equal to the modulus of the nth 3-dimensional block, normalized by a factor $\sqrt{N}$.

In a more general scenario, the skews are due to the presence of multiplexers at both the input and output of the system setup; therefore, the measured transfer matrix $\mathbf{T}$ takes the form

$$\mathbf{T} = \mathbf{M}_{\text{out}}\mathbf{F}\,\mathbf{M}_{\text{in}}, \tag{6}$$

where $\mathbf{M}_{\text{in}}$ and $\mathbf{M}_{\text{out}}$ are block-diagonal matrices accounting for scalar and polarization delays due to the fan-in and fan-out optical networks, respectively, and $\mathbf{F}$ is the matrix of the SDM fiber. Assuming for simplicity that there is no MDL, the MD vector $\vec{\tau}_T$ associated to $\mathbf{T}$ can be written as [5]

$$\vec{\tau}_T(\omega) = \vec{\tau}_{\text{out}} + e^{\omega(\vec{\tau}_{\text{out}}\times)}\vec{\tau}(\omega) + e^{\omega(\vec{\tau}_{\text{out}}\times)}\mathbb{F}(\omega)\,\vec{\tau}_{\text{in}}, \tag{7}$$

where $\vec{\tau}_{\text{out}}$ and $\vec{\tau}_{\text{in}}$ are the MD vectors containing information about the output and input skews, respectively, $\vec{\tau}$ is the MD vector of the SDM fiber only, and $\mathbb{F}$ is the generalized Müller matrix associated with $\mathbf{F}$. The MD vectors $\vec{\tau}_{\text{in}}$ and $\vec{\tau}_{\text{out}}$ describe deterministic scalar and polarization delays, therefore they are constant in frequency. Differently, the MCF link operates in a strong mode mixing regime and hence exhibits a random spectral behavior. As a consequence, the frequency average of the second and last terms of (7) is to a good approximation equal to zero. A similar conclusion holds also for moderate MDL. Indeed, the vector $\vec{\tau}$ and the matrix $\mathbb{F}$ have a frequency structure that is statistically independent of $\vec{\tau}_{\text{in}}$ and $\vec{\tau}_{\text{out}}$. While $\vec{\tau}$ characterizes the properties of the SDM fiber, $\vec{\tau}_{\text{in}}$ and $\vec{\tau}_{\text{out}}$ describe the fan-in and fan-out networks, respectively. As a result, with a very good

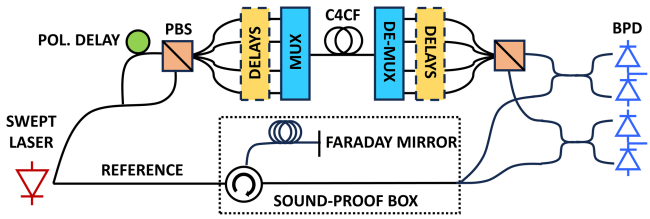

Fig. 1. Experimental setup for swept-wavelength characterization of deployed multi-core fiber (after [16]).

approximation we have

$$\vec{\tau}_{\text{out}} \approx \langle \vec{\tau}_T(\omega) \rangle \,, \tag{8}$$

where the average is perform with respect to frequency.

The measurement of the transfer matrix $\mathbf{T}$ allows to calculate with a similar procedure also $\vec{\tau}_{\text{in}}$. Owing to the reciprocity theorem [14], [15], the transfer matrix $\mathbf{B}(\omega)$ describing backward propagation is $\mathbf{B} = \mathbf{T}^T = \mathbf{M}_{\text{in}}^T \mathbf{F}^T \mathbf{M}_{\text{out}}^T$. The associated MD vector $\vec{\tau}_B(\omega)$ has the same structure as in (7), with the subscripts "in" and "out" swapped. By the same arguments given above, we therefore find $\vec{\tau}_{\text{in}} \approx \langle \vec{\tau}_B(\omega) \rangle$.

The above procedure allows to isolate the transmission matrix of the SDM fiber from the measured matrix $\mathbf{T}$. Using the derived $\vec{\tau}_{\text{in}}$ and $\vec{\tau}_{\text{out}}$, we construct the corresponding matrices $\mathbf{M}_{\text{in}}$ and $\mathbf{M}_{\text{out}}$:

$$\mathbf{M}_* = \exp\left(-i \frac{\vec{\tau}_* \cdot \vec{\mathbf{\Lambda}}}{2\,N} \omega \right), \quad \text{with} * = (\text{in, out}) \tag{9}$$

Once the two skew matrices have been computed, we can calculate the transfer matrix of the SDM fiber alone as $\mathbf{F} = \mathbf{M}_{\text{out}}^{-1} \mathbf{T} \mathbf{M}_{\text{in}}^{-1}$. This ensures accurate characterization of the SDM link.

III. Experimental Setup

The experimental data used in this article are obtained from a field-deployed coupled-core four-core fiber (C4CF) link [17]. The cable has a length of 6.3 km. It is installed in an underground tunnel and includes (among the others) 12 strands of C4CF. The link analyzed in this work is formed by concatenating 11 of these strands, resulting in a total length of about 69 km. The measured frequency-dependent MDL, as shown in [16], consistently remains below 3 dB across the entire 100 nm bandwidth, even though the link consists of 11 spliced segments.

The primary objective of the experiment is to measure the transfer matrix of the SDM system. An effective technique for directly measuring the transfer function matrix is based on swept wavelength interferometry (SWI) [18], which employs an interferometric setup wherein one arm contains a device under test (DUT) that is excited by a swept optical source. Leveraging DSP, the transfer function matrix can be extracted from the resulting fringe pattern. To measure the complete transfer function matrix in a single sweep, polarization diverse detection and a network of delay lines are incorporated into the setup [19], [20], [21]. The experimental setup is shown in Fig. 1. For the C4CF, accurately determining the transfer matrix requires coherent measurements of all the outputs originating from a given input. A detailed description of the experimental setup and data acquisition technique, can be found in [16].

IV. Statistical Analysis of Modal Dispersion

In the following, we report the statistical analysis of the measured modal dispersion. The first step is to calculate the MD matrix $\mathbf{Q}_T$ of the complete link from the values of $\mathbf{T}$ that are measured at the discrete frequencies ω_n. This is well approximated by the expression

$$\mathbf{Q}_T \approx -i \frac{\operatorname{logm}\left[\mathbf{T}(\omega_n) \mathbf{T}^{-1}(\omega_{n-k}) \right]}{\omega_n - \omega_{n-k}}, \tag{10}$$

where logm represents the matrix logarithm, and the value of k determines the frequency step used to compute the derivative of $\mathbf{T}$. In our calculations, we set $k = 4$, corresponding to a frequency step of 2 GHz. From $\mathbf{Q}_T$, we derive the generalized MD vector $\vec{\tau}_T$, which consists of the $D = 63$ complex-valued components shown in Fig. 2. Despite the link has an average MDL of about 2.9 dB, the magnitude of the imaginary part of $\vec{\tau}_T$ is significantly smaller (about two orders of magnitude) than the real part. For this reason in the following we focus on the real part of the MD vector.

As discussed in the previous section, the first 3 N components of $\vec{\tau}_T$ correspond to the delays among the polarization components of each spatial mode, while the last $N-1$ components of $\vec{\tau}_T$ are related to the delays between the spatial modes [5]. As it is evident from Fig. 2, these last three components have non-zero averages. Following the analysis made in Section II-A, these non-zero average values are due to the scalar delays $\vec{\tau}_{\text{out}}$ that appear in (7), which can be attributed to a non perfect compensation of the lengths of the delay network at the receiver side of the experimental setup. Similarly, by considering $\mathbf{T}^T$ and examining the reciprocal scenario, we can obtain the components of $\vec{\tau}_{\text{in}}$, highlighting the possible delays caused by the patch cords of the input network.

Fig. 3(a) and (b) show the D elements of $\vec{\tau}_{\text{in}}$ and $\vec{\tau}_{\text{out}}$, respectively, calculated by averaging $\vec{\tau}_B(\omega)$ and $\vec{\tau}_T(\omega)$. These values are obtained by averaging not only with respect to frequency, but also over the 100 measurements of the link taken at different times. The standard deviation of these averages is about 0.82 ps, and this small value is indicative of the remarkable stability of the deployed fiber link. In both Fig. 3(a) and (b), the last three components are associated to the scalar skews according to (5). Inverting this expression and setting the skew of the first core to 0 as a reference, the skews of the other cores range from a few ps to a few tens of ps, corresponding to differences in length of the order of millimeters. They are attributed to the presence of multiplexers and imperfections in the calibration of the delay network. However, these two effects are not physically distinguishable from each other. Despite being inseparable, it is highly unlikely that these skews originate from the fiber. Therefore, it is practically certain that they stem from the measuring apparatus. Additionally, in Fig. 3(a), we observe peaks in the first components of $\vec{\tau}_{\text{in}}$, which arise from the polarization delay incorporated into the setup (transmitter side) that may not have been perfectly calibrated. Nevertheless, as discussed in the

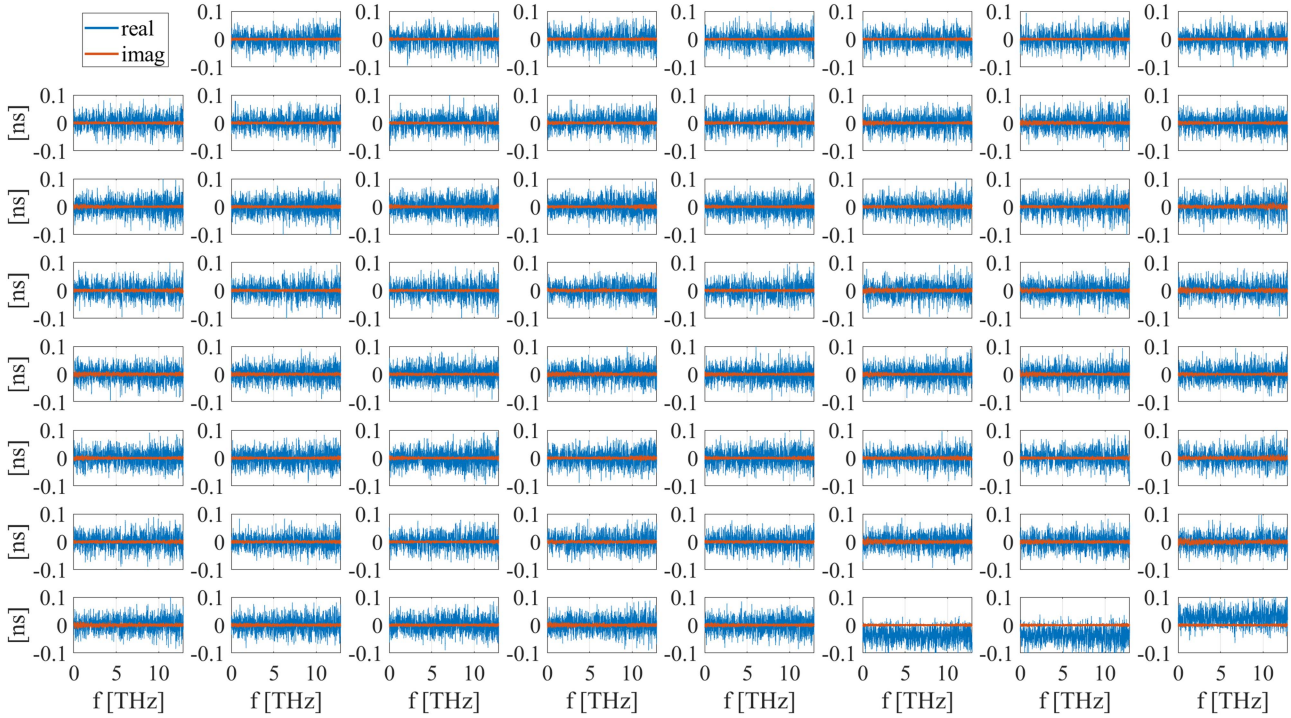

Fig. 2. Real and imaginary part of the $D = 63$ components of $\vec{\tau}_T$ as a function of the measurement frequency.

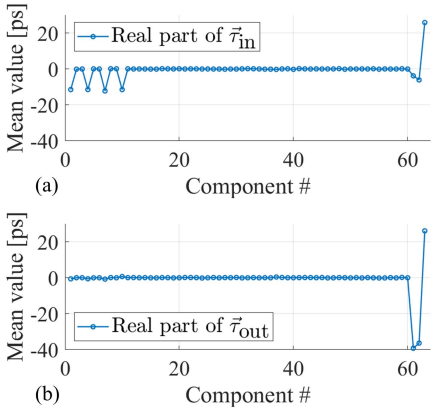

Fig. 3. (a) Computed values of the components of $\vec{\tau}_{\text{in}}$ and (b) $\vec{\tau}_{\text{out}}$.

previous section, once these skews have been measured, their effect can be removed from the transfer matrix, enabling the analysis of the MD affecting only the C4CF. This analysis is presented in the following sections.

A. Correlation of the Modal Dispersion Vector

The statistical properties of the MD vector $\vec{\tau}(\omega)$ of a fiber link in the long-length regime, i.e., in a condition of complete mode mixing, have been analyzed in [7]. Specifically, the two-frequency correlation functions of $\vec{\tau}$ are

$$r_{\vec{\tau},\vec{\tau}}(\Delta\omega) = \langle \vec{\tau}(\omega) \cdot \vec{\tau}(\omega + \Delta\omega) \rangle = \frac{D}{\Delta\omega^2} \left\{ 1 - \exp\left[-\frac{\tau^2 \Delta\omega^2}{D} \right] \right\}, \tag{11}$$

$$r_{\vec{\tau},\vec{\tau}^*}(\Delta\omega) = \langle \vec{\tau}(\omega) \cdot \vec{\tau}^*(\omega + \Delta\omega) \rangle = \frac{D\tau^2}{\Delta\omega^2\tau^2 - \alpha^2} \left\{ 1 - \exp\left[-\frac{\Delta\omega^2\tau^2 - \alpha^2}{D} \right] \right\}, \tag{12}$$

where the coefficients τ^2 and α^2 can be obtained by evaluating the correlations at $\Delta\omega = 0$ as follows:

$$\langle \vec{\tau} \cdot \vec{\tau} \rangle = \tau^2 \,, \qquad \langle \vec{\tau} \cdot \vec{\tau}^* \rangle = \frac{D\tau^2}{\alpha^2} \left(e^{\frac{\alpha^2}{D}} - 1 \right) . \tag{13}$$

Applying these formulas to the measured values of $\vec{\tau}$ (and recalling that $D = 63$), we find $\tau \approx 0.187$ ns and $\alpha \approx 1.717$. These values are used to compute the theoretical correlation given in (11) and (12), and the results are shown in Fig. 4 by the black dashed curves. In the same graphs, the solid lines are the real (blue) and imaginary (red) part of the experimental estimates of $r_{\vec{\tau},\vec{\tau}}(\Delta\omega)$ and $r_{\vec{\tau},\vec{\tau}^*}(\Delta\omega)$. The figure shows that there is an excellent agreement between theory and experiment: the real parts of the experimental correlation functions overlap with the plots of (11) and (12), while their imaginary parts are almost vanishing, consistently with the theory.

It is worthwhile remarking that the theoretical expressions (11) and (12) are real, regardless of whether the link has MDL or not, despite the MD vector $\vec{\tau}$ is complex in the latter case. As a further check of the consistency of the experimental data with the theory, we recall that the parameter α is related to the average MDL through [7]

$$\langle \text{MDL}_{\text{dB}} \rangle = g(N) \cdot \alpha \,, \tag{14}$$

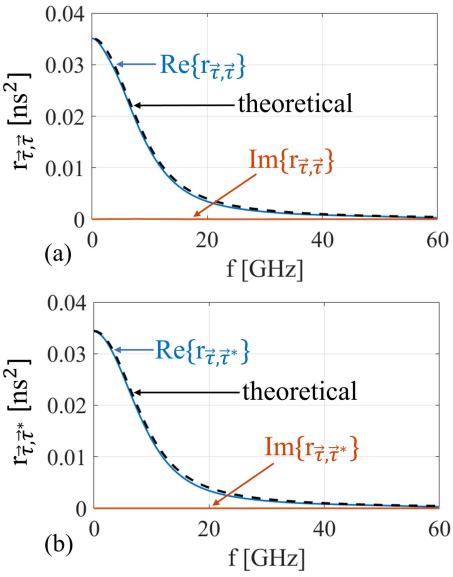

Fig. 4. Real and imaginary part of the autocorrelation functions (a) $\langle \vec{\tau} \cdot \vec{\tau} \rangle$ and (b) $\langle \vec{\tau} \cdot \vec{\tau}^* \rangle$ versus frequency. The dashed black lines refer to the theoretical expressions in (11) and (12).

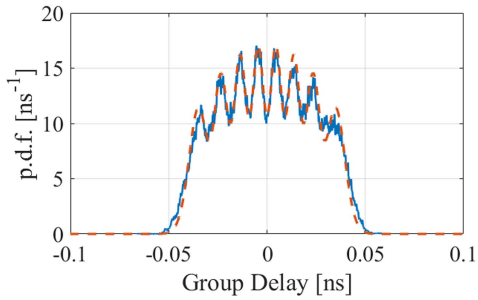

Fig. 5. Marginal PDF of the GDs. Solid blue curve: experimental estimate; dashed red curve: theoretical expression.

where $g(N)$ is a coefficient (with a cumbersome expression given in [7]) that depends only on the number of propagating spatial modes. In the present case $g(4) \approx 1.69$, which for $\alpha \approx 1.717$ yields $\langle \mathrm{MDL_{dB}} \rangle \approx 2.9$ dB, in good agreement with the measurement reported in [16].

B. Group Delay Analysis

Another important information that can be retrieved from the MD matrix, $\mathbf{Q}$, are the group delays (GD) of the principal propagating modes [22], [23], which are the real part of the eigenvalues of $\mathbf{Q}$. Fig. 5 shows the experimental marginal PDF, with the characteristic eight peaks associated to the eight principal states. The result is in very good agreement with the theoretical expression (shown by the dashed curve) reported in [23], despite this has been calculated under the assumption of no MDL. Analyzing the statistical properties of each single GD is not as straightforward, because in general the eigenvalues of $\mathbf{Q}$ do not have a natural sorting with respect to frequency. Nevertheless, in the strong mode coupling regime the joint PDF of the GDs is always zero whenever any two GDs are equal (see

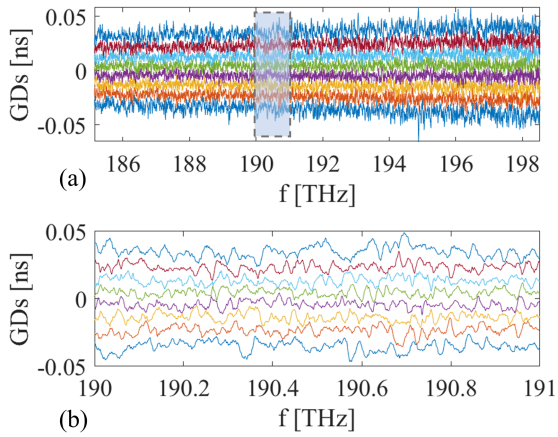

Fig. 6. (a) Experimental GDs as a function of frequency. (b) Zoomed-in view of the shadowed area.

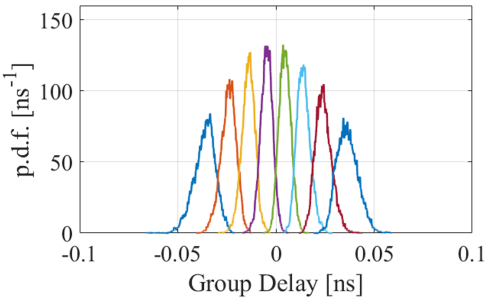

Fig. 7. PDFs of the individual GDs. Colors correspond to the ones used in Fig. 6.

Eq. (16) in [22]). This implies that the trajectories of the GDs as a function of frequency do not cross each other, and can be drawn by sorting (with respect to their real part) the eigenvalues of $\mathbf{Q}$ at each frequency. Fig. 6(a) shows the sorted GDs as a function of frequency over the whole measurement band, while Fig. 6(b) shows a zoomed-in portion of the graph. Indeed, these experimental curves provide a qualitative confirmation that in strong mode coupling regime GD trajectories do not cross each other. As a further support, Fig. 7 shows the PDF of the individual GDs. While we are not aware of analytical expressions for these PDFs, they resemble the analytical result obtained for lower numbers of modes [22], [23].

V. Properties of Transfer Matrix $\mathbf{F}$

Once the effect of the patch-cords used in the experimental setup is removed as described in Section II-A, the extracted matrix $\mathbf{F}$ can be used to evaluate the fiber IIR [9], which provides a convenient description of the mode dispersion properties of the fiber. In principle, the IIR of a fiber is determined by launching a frequency-flat broadband signal into the fiber, exciting only one mode, and measuring the total output power by summing the powers across all the modes. By sequentially exciting different modes and averaging the received power signals, we obtain the quantity of interest, denoted as $I(t)$. Mathematically, $I(t)$ can

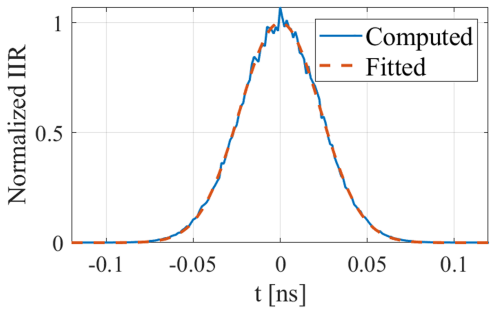

Fig. 8. Comparison of the experimental IIR (solid line) with the theoretical expression (dashed line) from (16).

be expressed as:

$$I(t) = \frac{1}{2\,N}\text{Trace}[\mathbf{H}(t)\mathbf{H}^{\dagger}(t)], \tag{15}$$

where $\mathbf{H}(t)$ represents the inverse Fourier transform of the transfer matrix $\mathbf{F}(\omega)$. In the regime of strong mode mixing, the average IIR is given by [7]:

$$\tilde{I}(t) = I_0\ \exp\left(-\frac{2\,N^2 t^2}{\tau^2}\right), \tag{16}$$

where I_0 is a normalization constant accounting for gain and loss, and τ is the same RMS GD introduced in (13).

Fig. 8 shows the normalized IIR calculated from the experimental data (solid curve), and the best fitting theoretical curve according to (16) (dashed curve); the two curves have an excellent agreement. The best fitting is obtained for $\tau \approx 0.185$ ns, which is in very good agreement with the measure of τ provided by the analysis of the correlation functions (see Section IV-A).

VI. Conclusion

We reported an extensive experimental characterization of the statistical properties of the MD of a field-deployed MCF link. The analysis of the complex MD vector enables a clear characterization of the skews of the optical link. We have also described a procedure to remove the effects of these skews when they are caused by the input or output multiplexers. This correction process along with the subsequent analyses of intensity impulse response and modal group delays, highlights the remarkable accuracy of the statistical model of MD in strong mode coupling regime. These results provide insights for further optimization and design of SDM transmission systems using multi-core fibers, with the potential to improve fiber-optic communication capacity and performance.

Appendix
Random Coupling Model

The propagation of light through an optical fiber is described by a linear operator $\mathbf{F}(z,\omega)$, such that

$$\vec{E}(z,\omega) = \mathbf{F}(z,\omega)\vec{E}(0,\omega). \tag{17}$$

When considering the propagation in the frequency domain, $\mathbf{F}(z,\omega)$ can be conveniently represented by a $2\,N \times 2\,N$ frequency-dependent matrix, unitary at each frequency in the absence of MDL. The frequency evolution of $\mathbf{F}(z,\omega)$ has been detailed in Section (II), while its spatial evolution can be expressed as

$$\frac{\partial \mathbf{F}(z)}{\partial z} = i\mathbf{B}(z)\mathbf{F}(z). \tag{18}$$

where $\mathbf{B}(z)$ is a frequency-dependent Hermitian matrix representing the coupling among the propagating modes. Extending the Pauli-matrix formalism to model the multi-mode propagation yields [5]

$$\mathbf{B}(z) = \frac{\beta_0\mathbf{I} + \vec{\beta}\cdot\vec{\mathbf{\Lambda}}}{2\,N}, \tag{19}$$

with the dependence of β_0 and $\vec{\beta}$ on z and ω suppressed for simplicity. Notably, β_0 introduces a phase delay common to all the propagation modes, which is immaterial to our MD study and, therefore, can be set to zero. The vector $\vec{\beta}$ is a generalization of the birefringence vector, as it describes the local coupling among the various modes. Similar to the components of $\vec{\tau}$, the first N triplets of the components of $\vec{\beta}$ correspond to the birefringence vectors of the N individual propagation modes, while the remaining components represent coupling among the spatial modes. In [7], the statistical properties of MD have been studied describing the mode coupling vector $\vec{\beta}(z)$ as white Gaussian noise. In principle, the applicability of the white noise model holds when the correlation length of the mode coupling vector is significantly smaller than the overall system length, which is the case analyzed in this work. Using this assumption implies that the distribution of $\mathbf{F}$ is independent of ω and that the statistics of the two-frequency product $\mathbf{F}^{\dagger}(z,\omega_1)\mathbf{F}(z,\omega_2)$ depends only on the frequency difference $\omega_2 - \omega_1$. These properties serve to demonstrate the wide-sense stationarity of the matrix $\mathbf{F}$ with respect to frequency, a well-established concept in the context of PMD studies in SMF systems [24].

References

[1] R.-J. Essiambre, G. Kramer, P. J. Winzer, G. J. Foschini, and B. Goebel, "Capacity limits of optical fiber networks," *J. Lightw. Technol.*, vol. 28, no. 4, pp. 662–701, Feb. 2010.
[2] P. J. Winzer, "Spatial multiplexing in fiber optics: The 10x scaling of metro/core capacities," *Bell Labs Tech. J.*, vol. 19, pp. 22–30, 2014.
[3] G. Rademacher et al., "High capacity transmission in a coupled-core three-core multi-core fiber," *J. Lightw. Technol.*, vol. 39, no. 3, pp. 757–762, Feb. 2021.
[4] R. Ryf et al., "High-spectral-efficiency mode-multiplexed transmission over graded-index multimode fiber," in *Proc. Eur. Conf. Opt. Commun.*, 2018, pp. 1–3.
[5] C. Antonelli, A. Mecozzi, M. Shtaif, and P. J. Winzer, "Stokes-space analysis of modal dispersion in fibers with multiple mode transmission," *Opt. Exp.*, vol. 20, no. 11, pp. 11718–11733, May 2012. [Online]. Available: https://opg.optica.org/oe/abstract.cfm?URI=oe-20-11-11718
[6] K.-P. Ho and J. M. Kahn, "Mode-dependent loss and gain: Statistics and effect on mode-division multiplexing," *Opt. Exp.*, vol. 19, no. 17, pp. 16612–16635, Aug. 2011. [Online]. Available: https://opg.optica.org/oe/abstract.cfm?URI=oe-19-17-16612
[7] C. Antonelli, A. Mecozzi, M. Shtaif, N. K. Fontaine, H. Chen, and R. Ryf, "Stokes-space analysis of modal dispersion of SDM fibers with mode-dependent loss: Theory and experiments," *J. Lightw. Technol.*, vol. 38, no. 7, pp. 1668–1677, Apr. 2020.

[8] T. Hayashi, Y. Tamura, T. Hasegawa, and T. Taru, "Record-low spatial mode dispersion and ultra-low loss coupled multi-core fiber for ultra-long-haul transmission," *J. Lightw. Technol.*, vol. 35, no. 3, pp. 450–457, Feb. 2017.

[9] A. Mecozzi, C. Antonelli, and M. Shtaif, "Intensity impulse response of SDM links," *Opt. Exp.*, vol. 23, no. 5, pp. 5738–5743, Mar. 2015. [Online]. Available: https://opg.optica.org/oe/abstract.cfm?URI=oe-23-5-5738

[10] M. Cappelletti et al., "Statistical characterization of modal dispersion in field-deployed multi-core fiber," in *Proc. Eur. Conf. Opt. Commun.*, 2023, pp. 1–4.

[11] C. Antonelli et al., "The city of L'aquila as a living lab: The INCIPICT project and the 5G trial," in *Proc. IEEE 5G World Forum*, 2018, pp. 410–415.

[12] S. Fan and J. M. Kahn, "Principal modes in multimode waveguides," *Opt. Lett.*, vol. 30, no. 2, pp. 135–137, Jan. 2005. [Online]. Available: https://opg.optica.org/ol/abstract.cfm?URI=ol-30-2-135

[13] M. Shtaif and O. Rosenberg, "Polarization-dependent loss as a waveform-distorting mechanism and its effect on fiber-optic systems," *J. Lightw. Technol.*, vol. 23, no. 2, pp. 923–930, Feb. 2005.

[14] R. C. Jones, "A new calculus for the treatment of optical systemsvi. experimental determination of the matrix∗," *J. Opt. Soc. Amer.*, vol. 37, no. 2, pp. 110–112, Feb. 1947. [Online]. Available: https://opg.optica.org/abstract.cfm?URI=josa-37-2-110

[15] L. Palmieri, L. Schenato, M. Santagiustina, and A. Galtarossa, "Rayleigh-based distributed optical fiber sensing," *Sensors*, vol. 22, no. 18, pp. 2–7, 2022. [Online]. Available: https://www.mdpi.com/1424-8220/22/18/6811

[16] M. Mazur et al., "Transfer matrix characterization of field-deployed MCFs," in *Proc. Eur. Conf. Opt. Commun.*, 2020, pp. 1–4.

[17] T. Hayashi et al., "Field-deployed multi-core fiber testbed," in *Proc. 24th OptoElectronics Commun. Conf. Int. Conf. Photon. Switching Comput.*, 2019, pp. 1–3.

[18] D. K. Gifford, B. J. Soller, M. S. Wolfe, and M. E. Froggatt, "Optical vector network analyzer for single-scan measurements of loss, group delay, and polarization mode dispersion," *Appl. Opt.*, vol. 44, no. 34, pp. 7282–7286, Dec. 2005. [Online]. Available: https://opg.optica.org/ao/abstract.cfm?URI=ao-44-34-7282

[19] G. VanWiggeren and D. Baney, "Swept-wavelength interferometric analysis of multiport components," *IEEE Photon. Technol. Lett.*, vol. 15, no. 9, pp. 1267–1269, Sep. 2003.

[20] N. K. Fontaine et al., "Characterization of space-division multiplexing systems using a swept-wavelength interferometer," in *Proc. IEEE Opt. Fiber Commun. Conf. Expo. Nat. Fiber Optic Eng. Conf.*, 2013, pp. 1–3.

[21] S. Rommel et al., "Polarization equalization in optical vector network analysis for SDM fiber characterization," *IEEE Photon. Technol. Lett.*, vol. 31, no. 24, pp. 1917–1920, Dec. 2019.

[22] K.-P. Ho and J. M. Kahn, "Statistics of group delays in multimode fiber with strong mode coupling," *J. Lightw. Technol.*, vol. 29, no. 21, pp. 3119–3128, Nov. 2011.

[23] K.-P. Ho and J. M. Kahn, "Mode coupling and its impact on spatially multiplexed systems," in *Optical Fiber Telecommunications*. Amsterdam, Netherlands: Elsevier, 2013, pp. 491–568. [Online]. Available: https://linkinghub.elsevier.com/retrieve/pii/B9780123969606000110

[24] M. Shtaif and A. Mecozzi, "Study of the frequency autocorrelation of the differential group delay in fibers with polarization mode dispersion," *Opt. Lett.*, vol. 25, no. 10, pp. 707–709, May 2000. [Online]. Available: https://opg.optica.org/ol/abstract.cfm?URI=ol-25-10-707

Open Access funding provided by 'Università degli Studi di Padova' within the CRUI CARE Agreement